Available online at www.sciencedirect.com
ScienceDirect
International Journal of Thermal Sciences 46 (2007) 589–604
International Journal of Thermal Sciences
www.elsevier.com/locate/ijts

Entropy generation during the quasi-steady burning of spherical fuel particles

V. Raghavan [a,*], G. Gogos [a], V. Babu [b], T. Sundararajan [b]

[a] *Department of Mechanical Engineering, University of Nebraska-Lincoln, Lincoln, NE 68588, USA*
[b] *Department of Mechanical Engineering, Indian Institute of Technology Madras, Chennai 600036, India*

Received 21 April 2006; received in revised form 11 July 2006; accepted 18 July 2006

Available online 23 August 2006

Abstract

Entropy generation during the quasi-steady combustion of spherical liquid fuel particles has been presented in detail. The effects of freestream velocity, particle diameter, ambient temperature and gravity, on the entropy generation rate, have been discussed in detail. In the range of sub-critical freestream velocity, where an envelope flame is present, the entropy generation rate presents a minimum value. At a critical velocity, where the flame transition occurs, the entropy generation rate reaches a maximum value. Flame transition significantly affects the entropy generation rate, which suffers a sharp decrease in its value after the transition. Heat transfer and chemical reaction contribute almost equally to the total entropy generation rate. When normal gravity is considered in an upward flow configuration, there is an increase in the entropy generation rate as compared to the zero gravity case. The effect of gravity poses a complex variation pattern in the entropy generation rate, for a downward flow configuration. The entropy generation rate decreases with increasing ambient temperature. The entropy generation rate increases with the particle diameter. A correlation has been presented for the non-dimensional entropy generation number as a function of Froude number.

Keywords: Entropy generation; Quasi-steady combustion; Envelope flame; Wake flame; Chemical reaction

1. Introduction

Several investigators have studied the combustion characteristics of spherical fuel particles such as pulverized coal particles burnt in the boilers of power plants and in metallurgical furnaces, a spray of fuel droplets fired in oil-fired furnaces and in gas turbine combustors and many others. The combustion process in these examples is primarily diffusion controlled. Quasi-steady combustion models for the burning of stationary particles have been developed in the past, for pulverized solid fuel particles [1–3] and for isolated liquid fuel droplets [4–6], in which the transport processes inside the particles are neglected. These quasi-steady models are applicable for the low pressure burning of fuel particles, after the initial ignition and internal heating transients are over. Verification of the quasi-steady models has been carried out using the porous sphere experiment technique [7,8]. The effect of a convective flow field on the rate of burning of liquid droplets has been investigated by several authors in the past [9–12]. The existence of an envelope diffusion flame was assumed in these studies. Pope and Gogos [13] developed a quasi-steady model with a new multi-component diffusion formulation. Pope and Gogos [14] investigated the extinction of the flame in the front portion of an *n*-heptane droplet at a particular freestream velocity and have developed suitable correlations. Recently, Raghavan et al. [15] investigated the quasi-steady burning of spherical methanol particles in a mixed convective environment, for a wide range of Reynolds numbers. The burning characteristics in the presence of an envelope flame, transition flame and a wake flame have been presented in detail. The transition from envelope flame to a wake flame at a critical freestream velocity has been correlated as a function of freestream Reynolds number. Several of the above studies employed temperature dependent variable thermo-physical properties [9,10,13–15].

* Corresponding author. Current address: N104 Walter Scott Engineering Center, Mechanical Engineering, UNL, 68588, USA. Tel.: +1 402 472 2905; fax: +1 402 472 1465.
E-mail address: raghavan@unlserve.unl.edu (V. Raghavan).

1290-0729/$ – see front matter
doi:10.1016/j.ijthermalsci.2006.07.006

Nomenclature

Be	Bejan number	
C_p	specific heat	$\mathrm{J\,kg^{-1}\,K^{-1}}$
d	particle diameter	m
D	mass diffusivity in	$\mathrm{m^2\,s^{-1}}$
Fr	Froude number $(u_\infty/(gd)^{1/2})$	
g	acceleration due to gravity	$\mathrm{m\,s^{-2}}$
k	thermal conductivity	$\mathrm{W\,m^{-1}\,K^{-1}}$
MW	molecular weight	$\mathrm{kg\,kmol^{-1}}$
N_S	total entropy generation number	
Re	Reynolds number $(\rho u_\infty d/\mu)$	
R_u	universal gas constant	$\mathrm{J\,kmol^{-1}\,K^{-1}}$
S'''	total entropy generation rate per unit volume	$\mathrm{W\,m^{-3}\,K^{-1}}$
S	total entropy generation rate over the entire volume	$\mathrm{W\,K^{-1}}$
T	temperature	K
u_∞	freestream velocity	$\mathrm{m\,s^{-1}}$
u_x, u	axial velocity component	$\mathrm{m\,s^{-1}}$
u_r, v	radial velocity component	$\mathrm{m\,s^{-1}}$
x, r	axial and radial coordinates	m
Y	mass fraction	

Greek symbols

ΔH_R	heat of reaction	$\mathrm{J\,kg^{-1}}$
ρ	density	$\mathrm{kg\,m^{-3}}$
μ	coefficient of viscosity	$\mathrm{Ns\,m^{-2}}$
σ, τ	normal and shear stresses	$\mathrm{N\,m^{-2}}$
$\dot{\omega}$	reaction rate	$\mathrm{kg\,m^{-3}\,s^{-1}}$

Subscripts

i	species index
∞	free stream conditions
m	gas mixture
s	droplet surface
h	due to heat transfer
μ	due to viscous dissipation
m	due to mass transfer
Ch	due to chemical reaction
b	due to body force
c	due to the coupling between heat and mass transfer

Even though many analytical and numerical models are available in the literature for investigating the combustion characteristics of spherical fuel particles, not many are available for analyzing the entropy generation during the combustion process. It is obvious that during combustion process, very complex chemical and transport processes that are highly irreversible, take place simultaneously. These result in the release of chemical energy and the distribution of the same in the form of heat by convective and diffusive transport processes. The energy conversion process from chemical to heat is accompanied by an irreversible increase in entropy, which leads to a decrease in exergy (available energy or useful work that can be extracted from the system). In order to minimize the destruction of exergy, entropy generation rate should be as small as possible. The analysis of entropy generation becomes important, since, the rate of exergy destruction is related to the rate of entropy generation in a process [16–21]. To carry out such an investigation on the burning of spherical fuel particles, it is important to identify the sources of entropy generation in flames and to evaluate their relative strengths at different conditions. Taking into account sources like dissipation of thermal, mechanical and other forms of energy in premixed flames from a flat flame burner, an expression for the entropy generation rate has been reported by Arpaci and Selamet [22]. Dash and Som have investigated the transport processes and associated irreversibility issues in droplet combustion in a convective medium [23]. In their model, the instantaneous rate of entropy production and its variation with time have been determined from the simultaneous numerical solution of the entropy conservation equations for both the gas and liquid phases. The relative influences of parameters such as initial Reynolds number, ratio of the free stream to initial droplet temperature and ambient pressure on the entropy generation rate in the process of droplet combustion have been established. Second law analysis of the burning of a single droplet in a convective environment has been reported by Puri [24]. In this study, optimum transfer number for minimizing entropy generation in droplet combustion was obtained, which has been found to be directly proportional to the square of relative velocity and inversely proportional to the heat release and temperature difference between the droplet surface and the surrounding gas. Theoretical model for entropy balance and exergy analysis of the droplet combustion process has been developed by Hiwase et al. [25]. Thermodynamic irreversibility and second law analysis in spray combustion process, for different inlet pressure, temperature and swirl, has been performed by Datta and Som [26]. An investigation of entropy generation in a confined laminar diffusion flame has been presented by Datta [27]. This study has been carried out under normal gravity and it has been shown that buoyancy induced motion alter the entropy generation rate. Nishida et al. [28] analyzed the entropy generation and exergy loss during the combustion process. Effect of oxygen mass fraction on local entropy generation rate in a methane-air burner has been numerically studied by Yapici et al. [29]. Recently, effects of gravity on structure and entropy generation of confined laminar diffusion flames has been investigated by Datta [30], where it has been shown that the entropy generation due to heat transfer increases with the strength of the gravitational field and the entropy generation due to the chemical reaction and mass transfer remains unaltered.

The present study is focused on presenting the entropy generation during the quasi-steady combustion of spherical liquid fuel particles. Effect of forced convection, flame transition, gravity, ambient temperature and particle size on entropy generation rates have been discussed. The particle diameter has

been varied from 8 mm to 18 mm. The freestream velocity has been varied from 0.2 $\mathrm{m\,s^{-1}}$ to 2 $\mathrm{m\,s^{-1}}$. The ambient temperature has been varied from 300 K to 1250 K. The variation of entropy generation rate with the above parameters has been presented in detail. At low freestream velocities, flame envelopes the particle. As the freestream velocity is increased, the flame extinguishes in the front portion of the particle and stabilizes either in the boundary layer in the downstream of the particle or in the wake region of the particle [14,15]. The effect of the flame transition from envelope to wake flame on the entropy generation rate has been presented. The effects of gravity on upward and downward flow configurations [11,12,15,31], in which the buoyancy will aid and oppose the forced convective flow, respectively, are taken into account and the entropy generation rates for both the cases are presented in detail. A correlation has been developed for non-dimensional entropy generation rate as a function of Froude number. A brief description of the numerical model employed, entropy generation calculations and results with discussions have been presented in the subsequent sections.

2. Numerical model

The salient features of the numerical model are:

(a) non-orthogonal control volumes with semi-collocated mesh,
(b) generalized interpolation of all the flow and transport variables in a cell,
(c) finite rate chemistry, and
(d) detailed evaluation of thermo-physical properties based on local temperature and species concentrations.

Numerical results have been obtained for a range of mixed convective flow conditions. The simulations have been carried out with the following simplifications:

(1) The flow is laminar and axisymmetric.
(2) Ideal-gas mixture formulation is used to account for density variations with temperature and concentration. However, the incompressible flow solution methodology has been adopted to derive the pressure field, as the flow velocities are considerably less than the speed of sound.
(3) Only the gas phase region has been modeled in a decoupled manner, assuming no slip boundary condition at the particle surface and no liquid-phase heating effects are considered. These approximations are applicable to the low pressure burning of a fuel particle, during the quasi-steady burning period.
(4) Single component fuel undergoing complete combustion through a global reaction step has been considered. Only gas-phase combustion is studied, which amounts to assuming high fuel volatility.
(5) Chapman–Enskog description for binary gas mixtures has been used to evaluate thermo-physical properties such as thermal conductivity and viscosity. Piecewise polynomials in temperature have been used to evaluate specific heats and species enthalpies [32,33].
(6) Thermal radiation effects are neglected, which amounts to assuming a non-luminous flame, as the fuel employed is methanol.
(7) The partial pressure of vapor adjacent to the particle surface is assumed to be equal to the vapor pressure of the fuel at the interface temperature. Thus, the fuel mole fraction adjacent to the particle can be written using the Clausius–Clayperon equation.

Local evaporation velocity at particle surface has been evaluated using the fact that the total fuel mass flow rate at the surface is equal to the sum of the fuel mass flow rates due to convection and diffusion. A theoretical analysis incorporating the above assumptions can be employed primarily for modeling the quasi-steady burning of liquid fuel particles, and for the combustion of solid fuel particles to a limited extent (when combustion occurs in the gas phase alone). Details of the governing equations, boundary conditions, evaluation of thermo-physical properties and reaction rates and detailed solution procedure have been presented in Raghavan et al. [15] and Raghavan [34]. Numerical formulation and solution procedure have been briefly presented in Appendix A.

The local rate of generation of entropy per unit volume in a continuous domain involving mass, momentum and energy transfer along with chemical reaction and body forces due to buoyancy, can be described [16–25] as given below:

$$S''' = S'''_h + S'''_\mu + S'''_m + S'''_{\mathrm{Ch}} + S'''_b + S'''_c \tag{1}$$

where S''' represents the total entropy generated per unit volume ($\mathrm{W\,m^{-3}\,K^{-1}}$). The six terms in the right-hand side are the local entropy generation per unit volume due to heat transfer, viscous dissipation or fluid friction, mass transfer, chemical reaction, buoyancy-induced body force and the coupling between heat and mass transfer, respectively. They have been expressed in terms of temperature, velocity, mass fractions of species, reaction rate, gravitational force and temperature and concentration dependent thermo-physical properties, as presented below.

$$S'''_h = \frac{k}{T^2}\left(\left(\frac{\partial T}{\partial x}\right)^2 + \left(\frac{\partial T}{\partial r}\right)^2\right) \tag{2}$$

$$S'''_\mu = \frac{\mu}{T}\left\{2\left(\left(\frac{\partial u_x}{\partial x}\right)^2 + \left(\frac{\partial u_r}{\partial r}\right)^2 + \left(\frac{u_r}{r}\right)^2\right) + \left(\frac{\partial u_x}{\partial r} + \frac{\partial u_r}{\partial x}\right)^2\right\} \tag{3}$$

$$S'''_m = R_u \sum_i \frac{D_{i,m}\rho}{Y_i M W_i}\left\{\left(\frac{\partial Y_i}{\partial x}\right)^2 + \left(\frac{\partial Y_i}{\partial r}\right)^2\right\} \tag{4}$$

$$S'''_{\mathrm{Ch}} = \frac{(-\Delta H_R)\dot{\omega}}{T} \tag{5}$$

$$S'''_b = \frac{\rho u_\infty g}{T}\left(\frac{\rho_\infty}{\rho} - 1\right) \tag{6}$$

$$S'''_c = \frac{R_u}{T}\sum_i \frac{\rho D_{i,m}}{M W_i}\left\{\left(\frac{\partial Y_i}{\partial x}\frac{\partial T}{\partial x}\right)^2 + \left(\frac{\partial Y_i}{\partial r}\frac{\partial T}{\partial r}\right)^2\right\} \tag{7}$$

For the problem considered in the present study, viscous dissipation would be negligible and entropy generation due to viscous dissipation would be very small. The early reports on entropy generation during combustion process have indicated that the entropy generation due to body forces is negligible [27,30]. However, in order to quantitatively predict the order of magnitude of the entropy generation rates due to viscous dissipation and body force, contours of the same have been presented in a few cases.

The total entropy generation rate over the volume is calculated as follows:

$$S = \oint_V S'''(2\pi r \, \mathrm{d}r \, \mathrm{d}x) \tag{8}$$

Additionally, Bejan number (Be), which compares the magnitude of entropy generation rate due to heat transfer (S_h) to the total entropy generation rate (S), has been calculated as follows:

$$Be = \frac{S_h}{S} \tag{9}$$

A numerical code has been developed to calculate the entropy generation rates per unit volume and the overall entropy generation rate, presented in Eqs. (1)–(9) above. The results and discussion are presented in the next section.

3. Results and discussion

3.1. Effect of convective flow field

The flow configurations considered in this study are shown in Fig. 1. The upward flow configuration, where gravity-induced buoyancy effects will aid the forced convective field, is shown in Fig. 1(a). The downward flow configuration, where buoyancy-induced flow field opposes the forced convective flow field, is shown in Fig. 1(b). The effect of mixed convection on the entropy generation rate for both the configurations is presented in detail. Cases without the effects of gravity have also been discussed in order to bring out the effect of forced convection alone on the entropy generation rate.

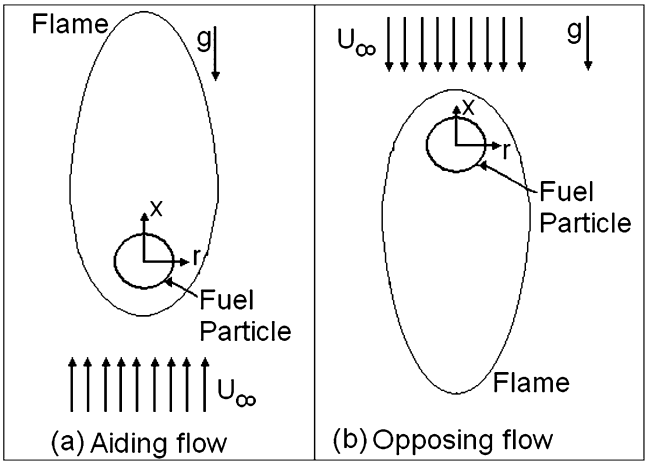

Fig. 1. Flow configurations considered in the present study.

For a methanol fuel particle burning in air in upward flow configuration under normal gravity with an ambient temperature of 300 K, at low free stream velocities, the flame envelopes the particle. The flame stand-off distance in the front portion of the particle decreases as the freestream velocity increases, although the shape of the flame in the rear region is almost unaffected [12,14,15,31]. When the freestream velocity is increased beyond a certain value called the critical velocity [15], transition from envelope to wake flame occurs. The critical velocity depends on the fuel employed, ambient temperature and particle diameter. After transition, there is no burning in the front portion of the sphere and the overall flame shape changes significantly [14,15,31]. Also, the fuel burning rate decreases due to the sudden decrease in the flame surface area [7,15,31]. As the freestream velocity is further increased, flame height is reduced [15]. Thus, there are two regimes of freestream velocities called the sub-critical regime, where an envelope flame is present and the super-critical regime, where either a transition flame or a wake flame is present.

Fig. 2 shows contours of the volumetric entropy generation rate for the case of an 8 mm fuel particle burning in air flowing with freestream velocity of 0.4 m s^{-1} and an ambient temperature of 300 K in an upward flow configuration under normal gravity. As discussed above, for the low freestream velocity considered here, an envelope flame is present around the particle. The maximum entropy generation rate per unit volume due to heat transfer occurs around the front stagnation point as shown in Fig. 2(a). The entropy generation rate due to viscous dissipation or fluid friction is very low (not shown here). Even though the maximum value of the volumetric entropy generation rate due to mass transfer (Fig. 2(b)) is greater than that due to heat transfer, the maximum value is localized around a very small area as indicated by contour value '11' in Fig. 2(b). Hence, the entropy generation rate integrated over the entire volume will be higher due to heat transfer than that due to mass transfer (discussed later along with Fig. 6). Volumetric entropy generation rate due to the coupling between heat and mass transfer contributes very little value to the total entropy generation rate (Fig. 2(c)). There is only negligible contribution to the entropy generation rate due to buoyancy-induced body force (Fig. 2(d)). Since, the strength of gravity-induced flow field is proportional to the non-dimensional gravity value ($(gd)^{1/2}/u_\infty$), when the freestream velocity is small as in the present case, gravity induced buoyancy effect is expected to be more pronounced. But, the body force does not seem to contribute to the entropy generation rate in this case. This is consistent with reports presented by previous researchers [21, 25,30].

Fig. 3 shows contours of the volumetric entropy generation rate due to chemical reaction (Fig. 3(a)) and contours of total entropy generation rate per unit volume (Fig. 3(b)) for the same case presented in Fig. 2. It is evident from Fig. 3 that chemical reaction contributes significantly to the total entropy generation rate. In a diffusion-controlled combustion, like the one occurring in this case, the rate of chemical reaction is much higher than the rates of diffusion of mass, momentum and heat. However, when the entropy generation rates due to diffusion

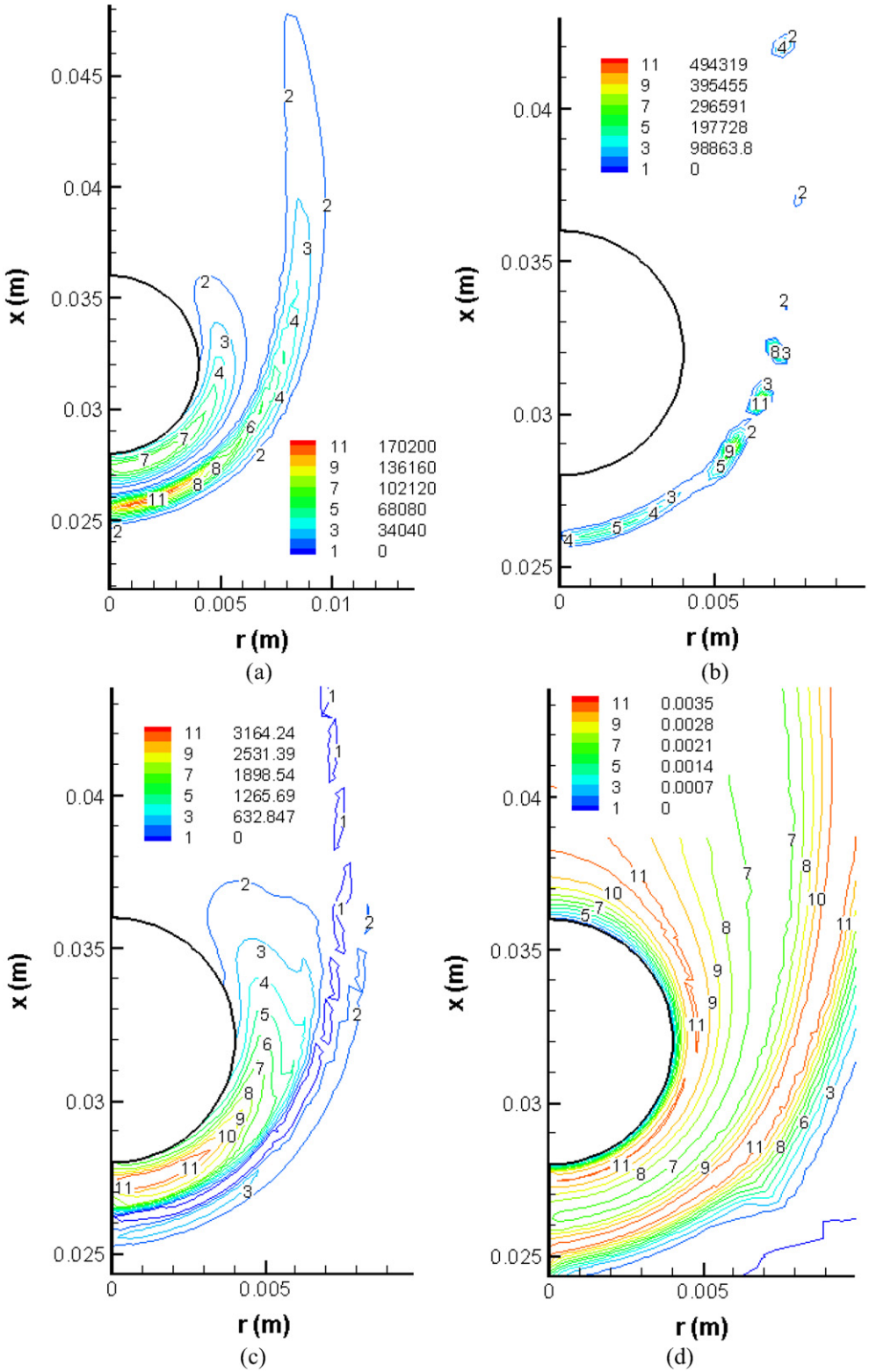

Fig. 2. Contours of local entropy generation rate in $W\,m^{-3}\,K^{-1}$, due to (a) heat transfer, (b) mass transfer, (c) coupling between heat and mass transfer and (d) body force due to gravity, for the case of an 8 mm particle burning in an upward flow configuration with freestream velocity of 0.4 $m\,s^{-1}$ and freestream temperature of 300 K, under normal gravity.

processes (heat and mass transfer) are combined, they exceed the entropy generation rate due to chemical reaction [25]. As in the case of entropy generation due to heat transfer (Fig. 2(a)), the maximum values in Fig. 3(a) occur around the front stagnation region. This is due to the fact that maximum fuel mass burning rate occurs at the front stagnation point, it decreases along the droplet surface and reaches a minimum value at the rear stagnation point [12]. Fresh air comes into contact with the

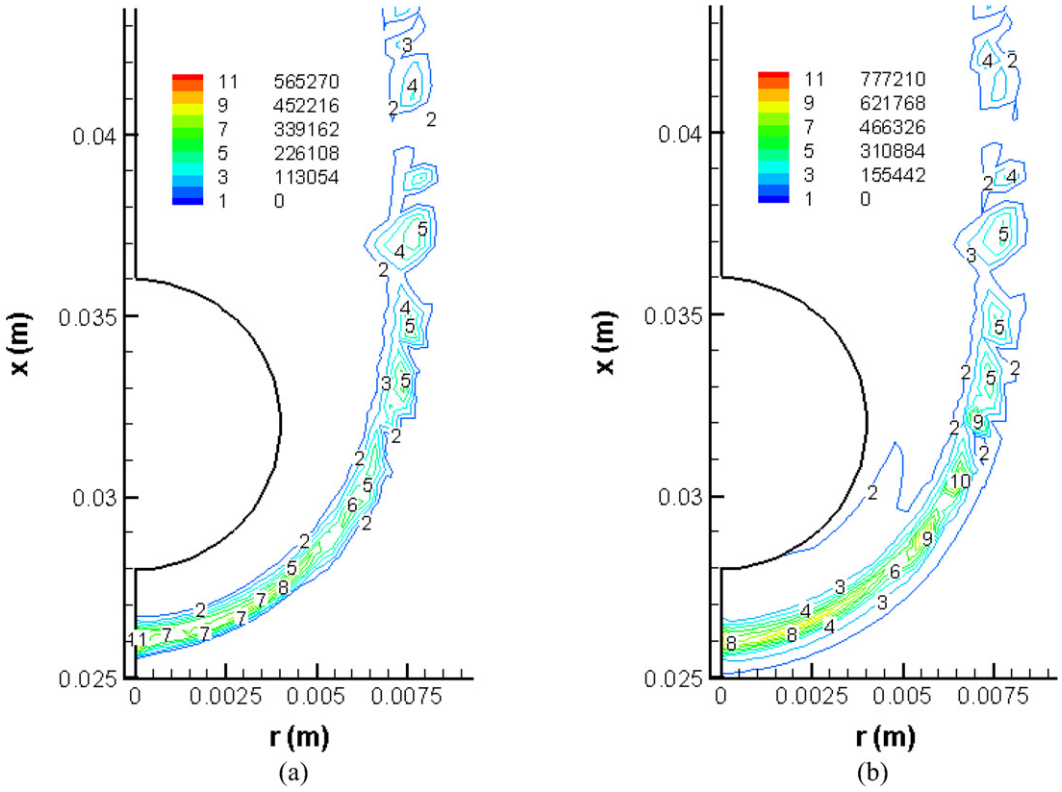

Fig. 3. Contours of (a) local entropy generation rate due to chemical reaction in $W\,m^{-3}\,K^{-1}$, and (b) total volumetric entropy generation in $W\,m^{-3}\,K^{-1}$, for the case of an 8 mm particle burning in an upward flow configuration with freestream velocity of $0.4\ m\,s^{-1}$ and freestream temperature of 300 K, under normal gravity.

fuel vapors around the front stagnation point and thus, rapid mixing and combustion take place here. Obviously, the entropy generation is also a maximum around this area.

To study the effect of flame transition on the entropy generation rate, a case with a higher freestream velocity ($1.5\ m\,s^{-1}$), which is in the super-critical regime for an 8 mm diameter particle burning in air in upward flow configuration at 300 K under normal gravity, has been considered. As discussed earlier, at this freestream velocity, extinction of the flame in the front portion of the particle occurs, because the flow residence time is less than the reaction time; in the wake region of the particle, where flow separation results in recirculation, flame is stabilized because of larger residence time for reactants [15]. After transition, combustion becomes partly diffusion-controlled and partly kinetics-controlled. Fig. 4 shows contours of the local entropy generation rate per unit volume for this case, where a transition flame (flame stabilized in the rear portion boundary layer of the particle) exists. Maximum values of the volumetric entropy generation rates due to heat transfer (Fig. 4(a)), mass transfer (not shown) and the coupling between heat and mass transfer (Fig. 4(c)) occur in a small region in the rear portion of the particle. Contribution to entropy generation rate due to mass transfer is about one-half of that due to heat transfer. There is very little contribution due to the coupling between heat and mass transfer (Fig. 4(c)), as reported in [21]. As in the previous case, contributions to entropy generation rate due to viscous dissipation (Fig. 4(b)) and body force (Fig. 4(d)) are negligible. Fig. 5(a) shows that the contribution to the volumetric entropy generation rate due to chemical reaction is significant in this case as well. Total volumetric entropy generation rate contours are presented in Fig. 5(b) for this case.

The variation of the entropy generation rate over the volume with freestream velocity, for the case of 8 mm fuel particle burning in an ambient of air at 300 K, under normal gravity is presented below. The variations of the total entropy generation rate integrated over the volume along with the contributions from heat transfer, mass transfer, chemical reaction and the coupling between heat and mass transfer are shown in Fig. 6. As discussed before, contributions to the entropy generation rate from viscous dissipation and body force are negligible and have not been presented here. The contribution from the coupling between heat and mass transfer is very little (shown by symbols in Fig. 6). For this particle diameter and ambient temperature, the transition from envelope flame to wake flame occurs at a freestream velocity around $0.9\ m\,s^{-1}$ [15]. Thus, a vertical line has been drawn in Fig. 6, dividing the sub-critical and super-critical freestream velocity regimes. It is evident from Fig. 6 that in the sub-critical regime, total entropy generation rate over the volume presents a minimum value around a freestream velocity of $0.4\ m\,s^{-1}$. The entropy generation due to chemical reaction also reaches a minimum value around this freestream velocity. However, it should be noted that the contribution from heat transfer gradually (linearly) increases with the freestream velocity (Fig. 6). The non-linear variation in entropy generation rate due to mass transfer is because of its dependence on the chemical reaction. Around the critical freestream velocity ($0.9\ m\,s^{-1}$), entropy generation over the volume reaches a maximum value. After transition, since the flame is put-off in

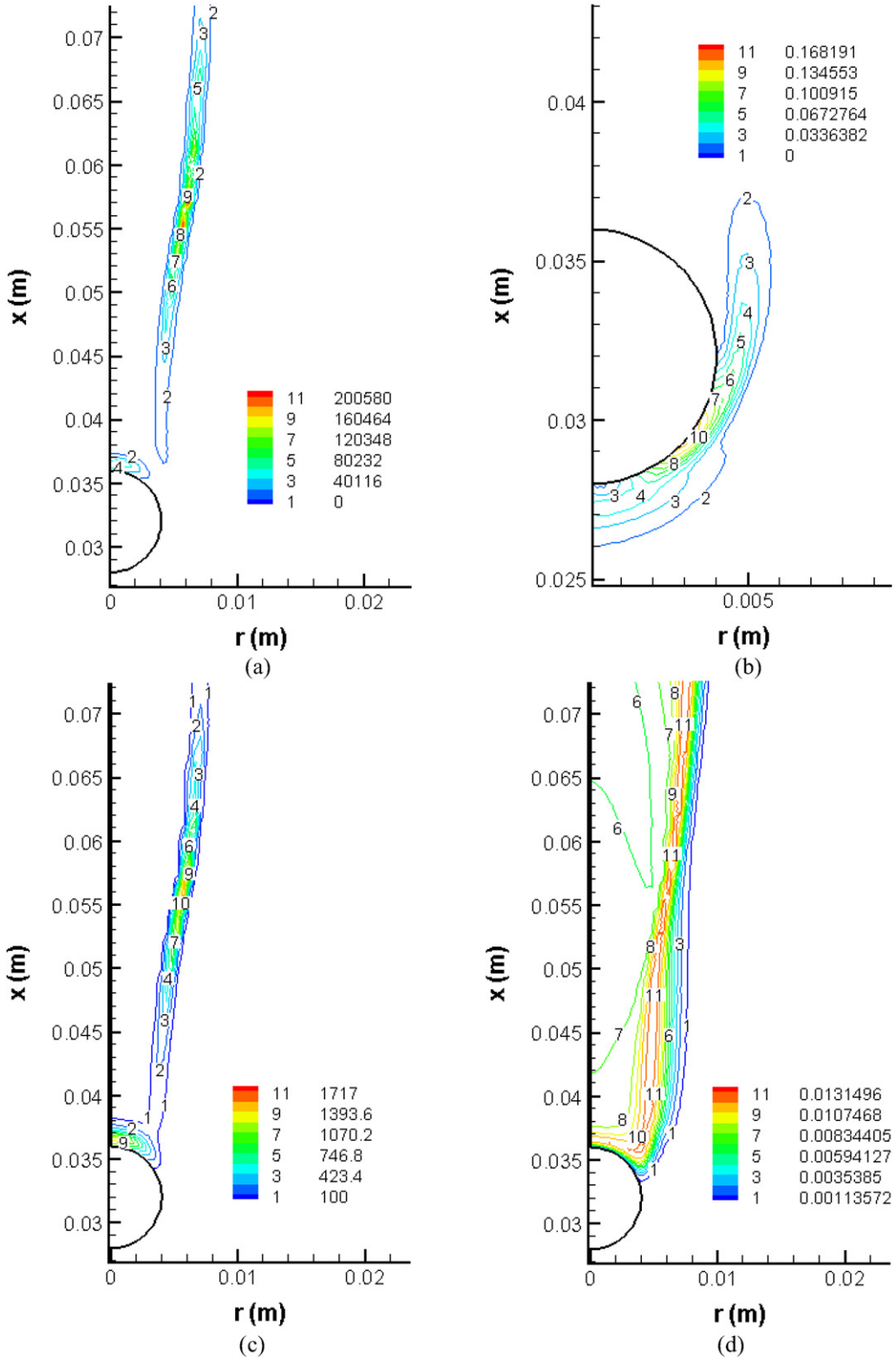

Fig. 4. Contours of local entropy generation rate in $W\,m^{-3}\,K^{-1}$, due to (a) heat transfer, (b) friction, (c) coupling between heat and mass transfer and (d) body force due to gravity, for the case of an 8 mm particle burning in an upward flow configuration with freestream velocity of 1.5 $m\,s^{-1}$ and freestream temperature of 300 K, under normal gravity.

the front portion of the particle, the flame surface area is reduced significantly. As a result, there is a sharp decrease in the integrated entropy generation rates as seen in Fig. 6. It should be noted that the fuel consumption rate also decreases sharply after transition [7,15]. After the sudden dip, entropy generation rates again increase with the freestream velocity. In the supercritical regime, till the freestream velocity values considered in the present study, entropy generation rates are smaller than

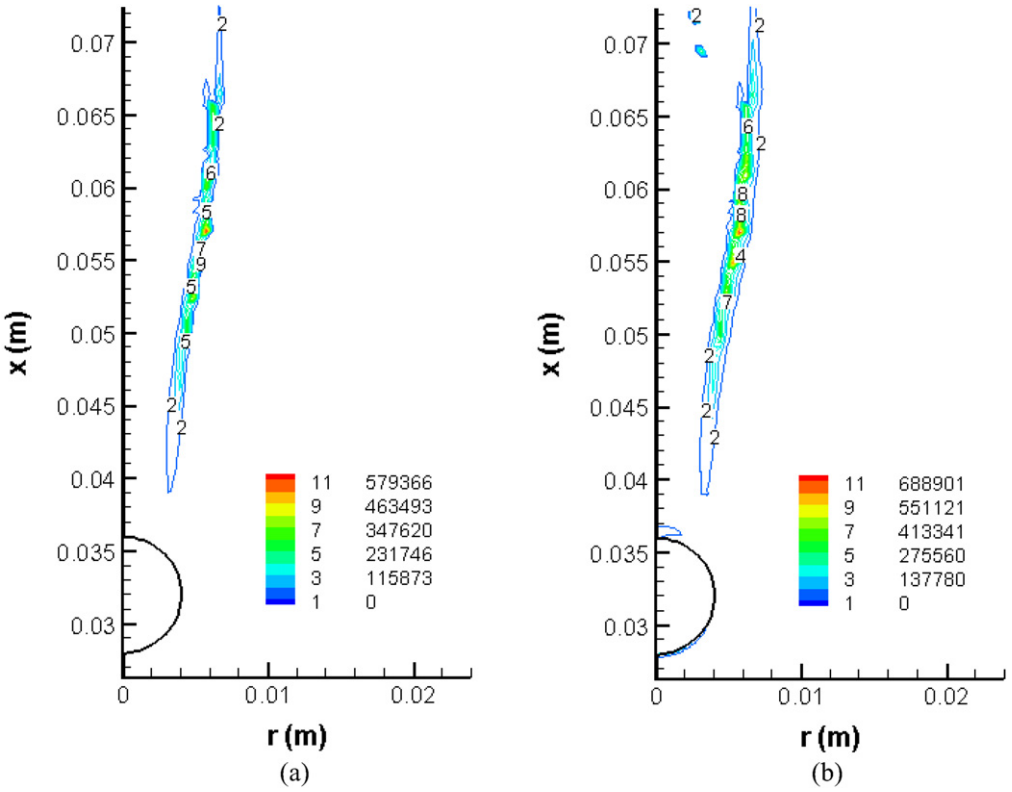

Fig. 5. Contours of (a) local entropy generation rate due to chemical reaction in $W\,m^{-3}\,K^{-1}$, and (b) total volumetric entropy generation in $W\,m^{-3}\,K^{-1}$, for the case of an 8 mm particle burning in an upward flow configuration with freestream velocity of 1.5 $m\,s^{-1}$ and freestream temperature of 300 K, under normal gravity.

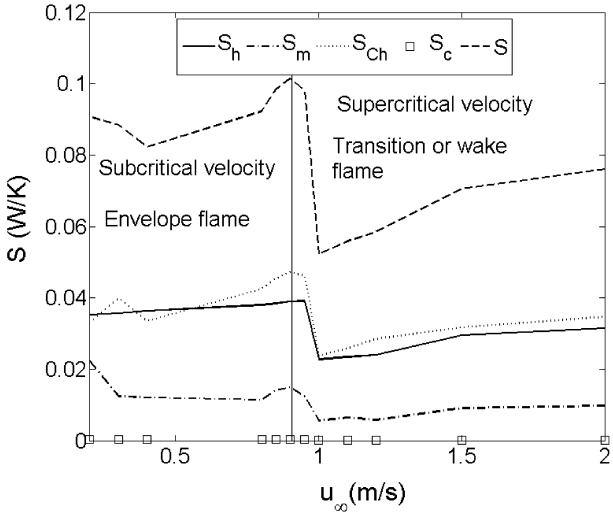

Fig. 6. Variation of the entropy generation rate over the volume ($W\,K^{-1}$) with freestream velocity, for the case of an 8 mm particle burning in an upward flow configuration with freestream temperature of 300 K, under normal gravity.

the minimum value of the sub-critical regime. However, in the super-critical regime where only a transition or a wake flame is present, the chance for the occurrence of incomplete combustion due to leakage of fuel is present.

To better understand the effect of buoyancy-induced flow on the entropy generation rate, cases for an 8 mm particle burning in upward and downward flow configurations under zero-gravity, at an ambient temperature of 300 K and different freestream velocities, have been simulated. Fig. 7 shows contours of entropy generation rate per unit volume due to heat transfer for zero gravity (Fig. 7(a)) and normal gravity (Fig. 7(b)), for an upward flow configuration with freestream velocity of 0.3 $m\,s^{-1}$. The flame stand-off distance from the particle surface is larger for the case under zero gravity than under normal gravity [12,15,31]. Contours of the volumetric entropy generation rate due to heat transfer reflect this fact. Since, in the upward flow configuration buoyancy-induced flow adds to the freestream convective flow, entropy generation rate for normal gravity is higher than that for zero gravity, which is consistent with the literature [27,30].

Fig. 8 presents the variation of the total entropy generation rate over the volume with freestream velocity for an 8 mm particle burning in air at 300 K in an upward flow configuration, under zero and normal gravity conditions. When the freestream velocity is less than approximately 0.4 $m\,s^{-1}$, total entropy generation rate over the volume increases with the freestream velocity for the case that neglects gravity and an opposite trend is observed for the case that includes gravity. It is evident from Fig. 8 that the entropy generation rate is higher when gravity is included [30]. The difference in entropy generation rates between both the cases is initially large at the lowest freestream velocity considered in the present study and the difference decreases with increasing freestream velocity. As mentioned earlier, the gravity-induced flow field has a higher strength at low freestream velocity and it decreases with increasing freestream velocity. This may be the reason for the case under normal gravity to have a decreasing trend in the entropy generation rate. The case under zero gravity experiences

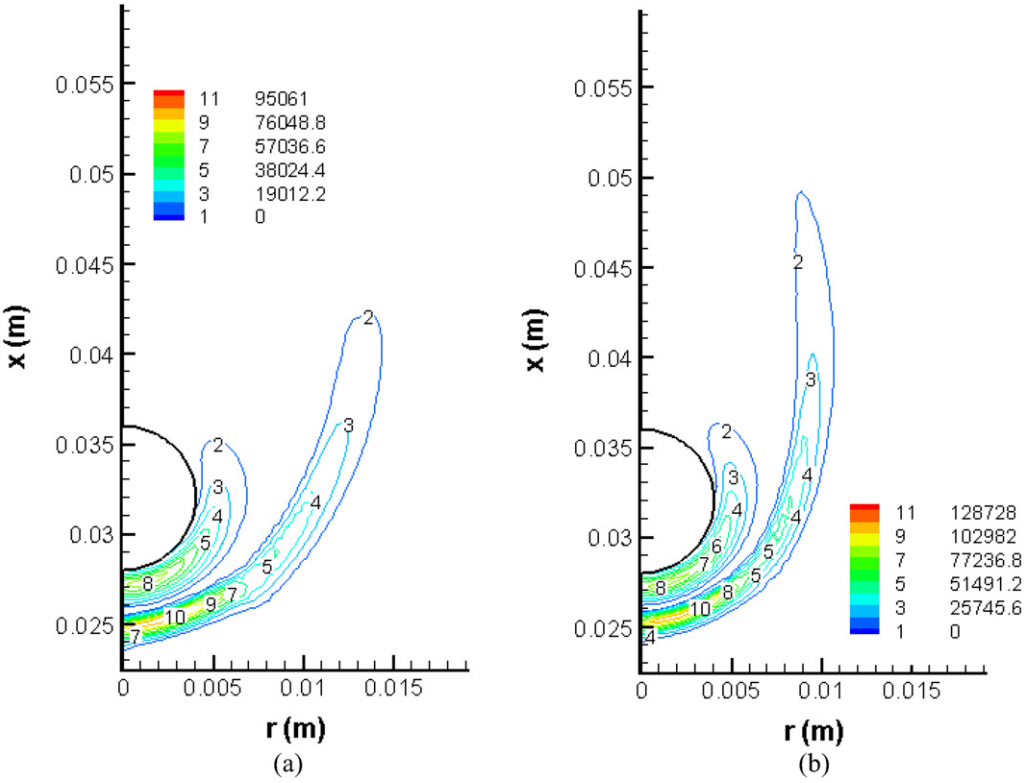

Fig. 7. Contours of the local entropy generation rate in $\mathrm{W\,m^{-3}\,K^{-1}}$ due to heat transfer, for the case of an 8 mm particle burning in an upward flow configuration with freestream velocity of 0.3 $\mathrm{m\,s^{-1}}$ and freestream temperature of 300 K, under (a) zero gravity and (b) normal gravity.

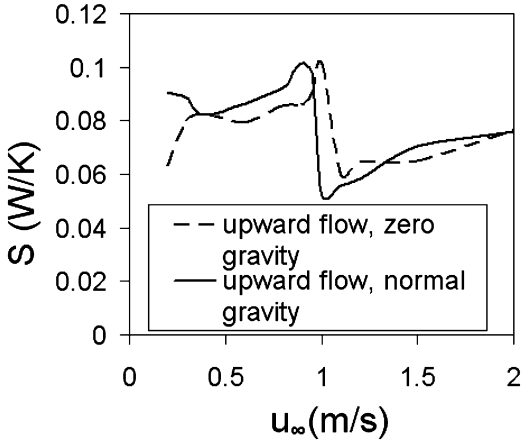

Fig. 8. Variation of the total entropy generation rate over the volume ($\mathrm{W\,K^{-1}}$) with freestream velocity, for the case of an 8 mm particle burning in an upward flow configuration under zero and normal gravity with freestream temperature of 300 K.

an increase in the convective strength due to the increase in the freestream velocity and this increases the entropy generation rate as well. When the freestream velocity is increased beyond 0.4 $\mathrm{m\,s^{-1}}$, an increasing trend in the entropy generation rate with freestream velocity is observed in both the cases, till flame transition occurs. The case under normal gravity experiences flame transition at a lower freestream velocity when compared to the case under zero gravity [31]. Thus, the sharp decrease in the entropy generation rate is observed at a lower freestream velocity for the case under normal gravity. After transition, the variation of the entropy generation rate in both the cases is almost similar. It can also be noted that, after transition, the difference in the total entropy generation rates over the volume between both the cases decreases as the freestream velocity increases and becomes nearly the same at the highest freestream velocity considered here. The decrease in the strength of the gravity-induced flow field due to the increase in the freestream velocity is the reason for this trend.

To study the opposing effect of buoyancy-induced flow field with respect to forced convection on entropy generation rate, a downward flow configuration for the burning of 8 mm particle has been considered under both zero and normal gravity. The ambient temperature is 300 K. Fig. 9 shows contours of total entropy generation rate per unit volume for both cases at a freestream velocity of 0.6 $\mathrm{m\,s^{-1}}$. At this freestream velocity, a laterally flattened flame shape that envelopes the particle is present for the case under normal gravity [31]. Thus, the maximum value of entropy generation rate occurs at a larger stand-off distance from the particle surface, for the case under normal gravity. In contrast to the upward flow configuration, the case under zero gravity has a higher value of entropy generation rate when compared to that under normal gravity, at this freestream velocity.

Total entropy generation rate over the volume has been plotted as a function of freestream velocity for the case of 8 mm particle burning in downward flow configuration under zero and normal gravity, in Fig. 10. For the case under normal gravity, at a low free stream velocity ($u_\infty \sim 0.2, 0.3\ \mathrm{m\,s^{-1}}$), the buoyancy effects dominate the forced convective field and the flame

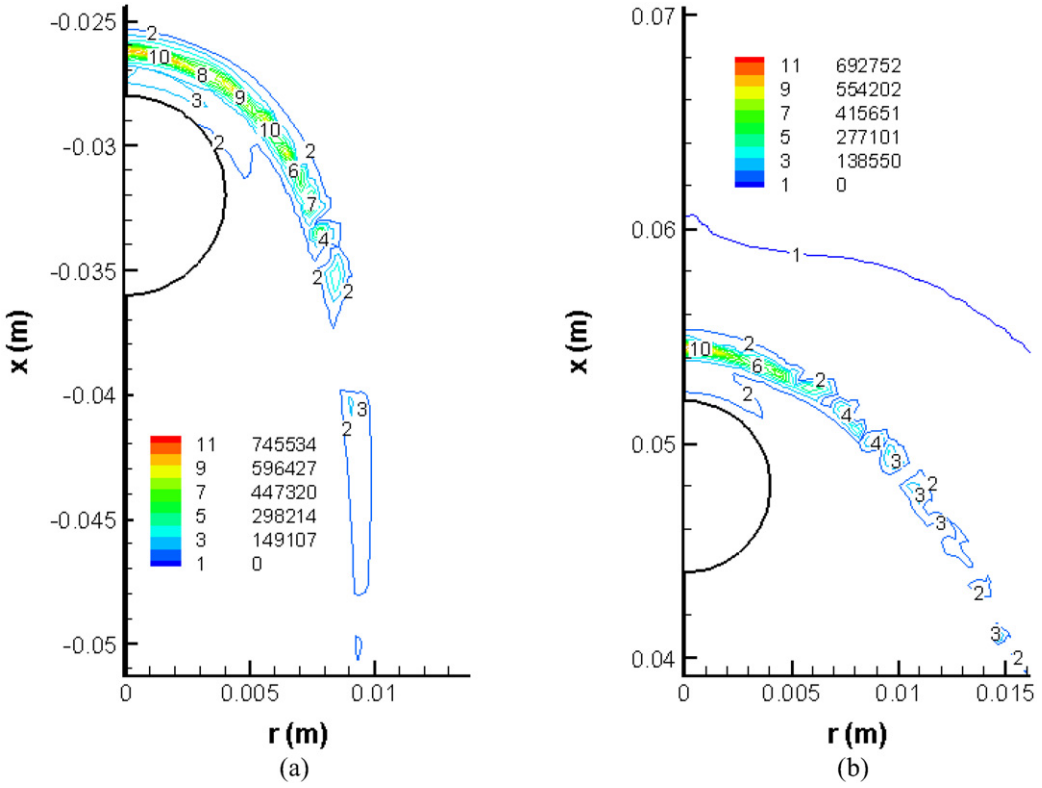

Fig. 9. Contours of the total entropy generation rate in W m^{-3} K^{-1}, for the case of an 8 mm particle burning in a downward flow configuration with freestream velocity of 0.6 m s^{-1} and freestream temperature of 300 K, under (a) zero gravity and (b) normal gravity.

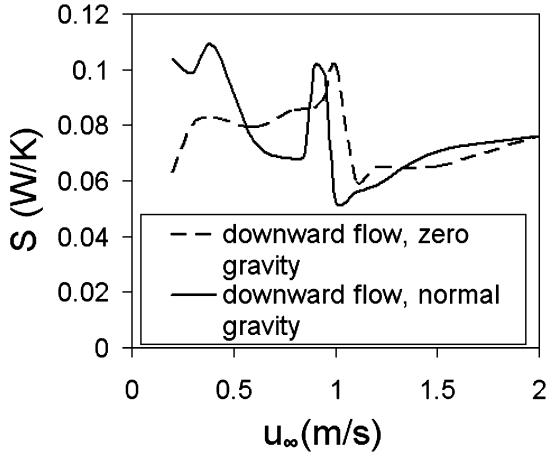

Fig. 10. Variation of the total entropy generation rate over the volume (W K^{-1}) with freestream velocity, for the case of an 8 mm particle burning in a downward flow configuration under zero and normal gravity with freestream temperature of 300 K.

extends in the upward direction [12,31]. As the freestream velocity is increased ($u_\infty \sim 0.4, 0.6$ m s^{-1}), the flame becomes laterally flattened and takes on a flat cylindrical shape [12, 31]. As the freestream velocity is increased further ($u_\infty \sim 0.8, 1.0, 1.1$ m s^{-1}), flame stand-off distances from the particle surface decrease and even at higher freestream velocity ($u_\infty \sim 1.2$ m s^{-1}), flame transition occurs [31]. A detailed comparison of the flame shapes and the mass burning rates between the cases under zero and normal gravity has been presented elsewhere [31]. The total entropy generation rate over the volume is higher for the case under normal gravity till the freestream velocity is less than approximately 0.4 m s^{-1}. As mentioned above, in this range of freestream velocity under normal gravity, the flame extends in an upward direction due to higher buoyancy strength. This higher buoyancy strength causes an increase in the entropy generation rate. When the flame becomes laterally flattened, which occurs when the freestream velocity is greater than approximately 0.5 m s^{-1} and less than approximately 0.8 m s^{-1}, entropy generation rate is lower for the case under normal gravity when compared to that under zero gravity. The total entropy generation rate integrated over the volume for the case under normal gravity decreases sharply at two different freestream velocities. First, a sharp decrease occurs around the freestream velocities in the range of 0.4–0.6 m s^{-1}, at which significant changes take place in the flame shapes. It should be noted that the fuel mass burning rate also decreases and reaches a minimum around a freestream velocity of 0.6 m s^{-1} [31]. There is also a sharp decrease in the entropy generation rate around freestream velocity of 1 m s^{-1}. Even though flame transition occurs for the case under normal gravity around a freestream velocity of 1.2 m s^{-1}, prior to the transition itself, a sharp decrease in entropy generation rate has been recorded. A sharp increase in entropy generation rate has also been observed around a freestream velocity of approximately 0.85 m s^{-1}. These variation trends, which are unusual when compared to those under zero gravity or for an upward flow configuration under zero and normal gravity, are due to the opposing effects of the buoyancy-induced flow field. Nevertheless, the contribution to the entropy generation rate from

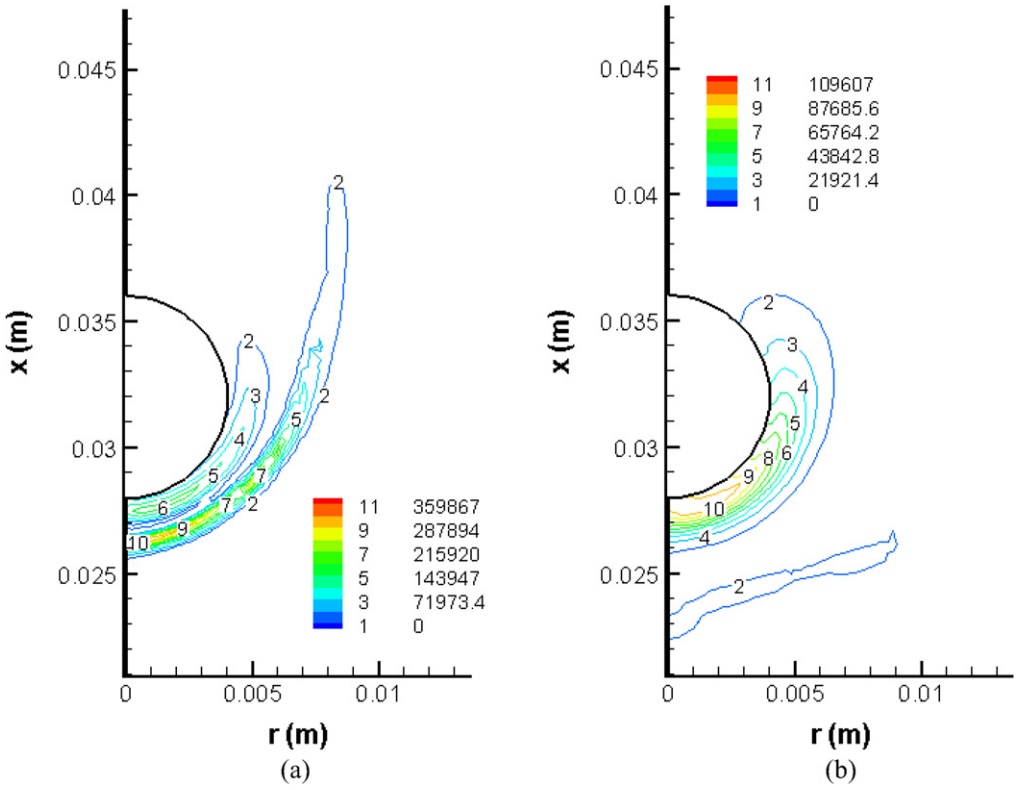

Fig. 11. Contours of the total entropy generation rate in $\mathrm{W\,m^{-3}\,K^{-1}}$ due to heat transfer, for the case of an 8 mm particle burning in an upward flow configuration with freestream velocity of 0.8 $\mathrm{m\,s^{-1}}$ and with freestream temperatures of (a) 300 K and (b) 1250 K.

body force is negligible for this case as well. Thus, it should be noted that the gravitational field considerably changes the flow field, flame shapes and fuel burning rates, and thus, the rate of entropy generation also, especially for the opposing flow case. After transition, the variation between the cases under zero and normal gravity become almost similar and the decrease in the buoyancy strength at higher freestream velocity is the reason for this trend.

3.2. *Effect of ambient temperature*

Cases for burning of an 8 mm particle in an upward flow configuration under normal gravity at different freestream velocities and ambient temperatures have been considered here. The ambient temperature has been varied from 300 K to 1250 K. Fig. 11 shows contours of volumetric entropy generation rate due to heat transfer at a free stream velocity of 0.8 $\mathrm{m\,s^{-1}}$, for the cases with ambient temperatures of 300 K and 1250 K. Localized maximum entropy generation near the front stagnation point has been observed for the case with $T_\infty = 1250$ K. It is evident from Fig. 11 that for the two ambient temperatures considered here, the entropy generation rate value is higher for the case with lower ambient temperature. This is consistent with results available in the literature [24,25,27].

Fig. 12 shows the variation of the entropy generation rate over the volume with freestream velocity, due to heat transfer (Fig. 12(a)), mass transfer (Fig. 12(b)) and chemical reaction (Fig. 12(c)). The variation of the total entropy generation rate is shown in Fig. 12(d). It should be noted that at high ambient temperatures (800 K and 1250 K), flame transition does not take place even at the maximum freestream velocity considered in the present study. In fact, the flame transition does not occur for the case with $T_\infty = 1250$ K, even till a freestream velocity of 10 $\mathrm{m\,s^{-1}}$ [15]. The entropy generation rate over the volume due to heat transfer has lower values at higher ambient temperatures (Fig. 12(a)) [25,27], except when the entropy generation rate for the lowest ambient temperature presents a minimum value due to flame transition. The case with $T_\infty = 800$ K, has altogether different trends in the variation of entropy generation rates due to mass transfer (dashed line in Fig. 12(b)), due to chemical reaction (dashed line in Fig. 12(c)), and thus, in the total entropy generation rate as well (dashed line in Fig. 12(d)). When the ambient temperature is 800 K, the rate of increase in the chemical reaction and the rate of increase in the diffusion of the species, in combination could have produced such a trend. Considering the cases with $T_\infty = 300$ K and 1250 K, the entropy generation rate due to chemical reaction has a lower value for the case with $T_\infty = 1250$ K, till flame transition takes place for the case with $T_\infty = 300$ K. The same trend is observed in the total entropy generation rate as well (Fig. 12(d)). The entropy generation rate due to mass transfer increases with

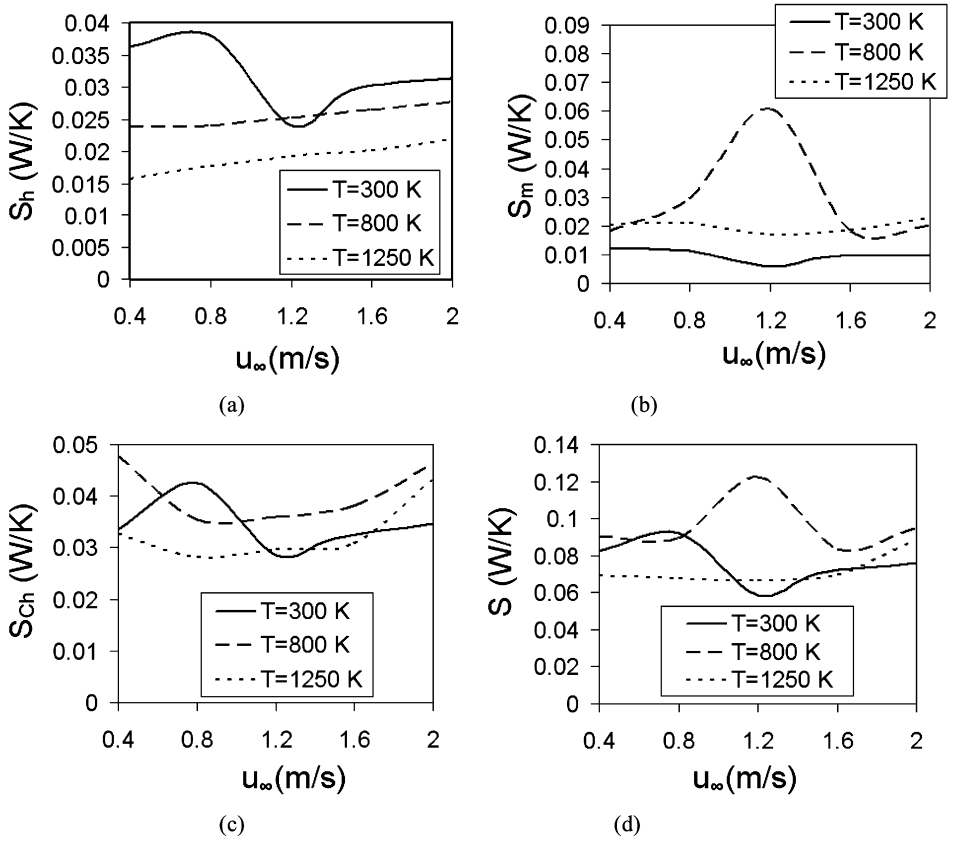

Fig. 12. Variations of the entropy generation rate over the volume ($\mathrm{W\,K^{-1}}$) with the freestream velocity, due to (a) heat transfer, (b) mass transfer, (c) chemical reaction and (d) total entropy generation rate, for the case of an 8 mm particle burning in an upward flow configuration at different freestream temperatures, under normal gravity.

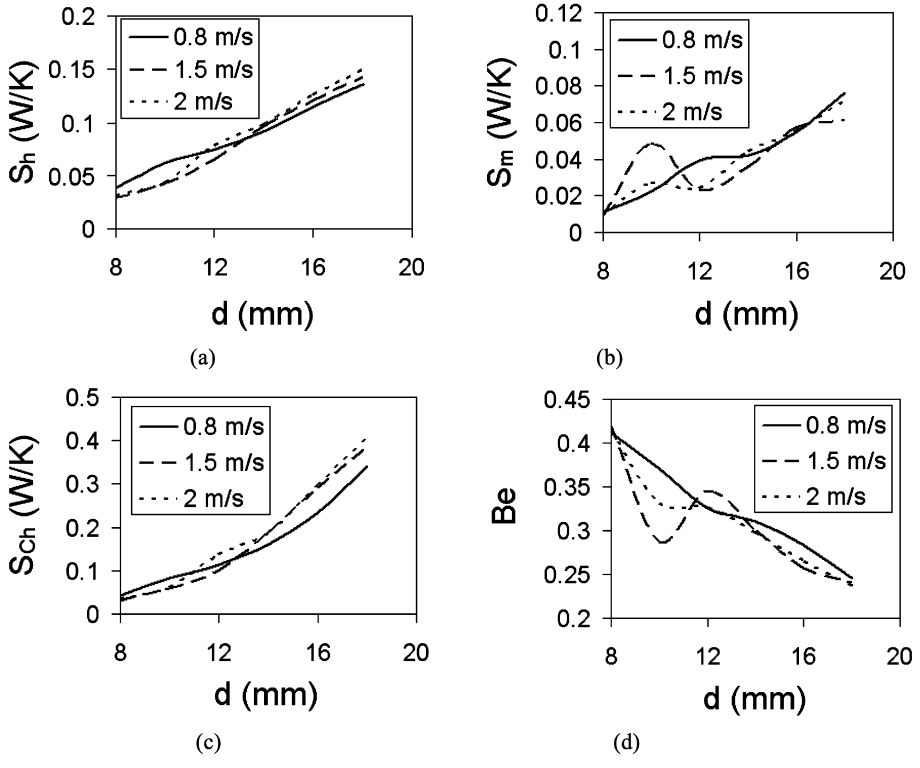

Fig. 13. Variations of the entropy generation rate over the volume ($\mathrm{W\,K^{-1}}$) due to (a) heat transfer, (b) mass transfer, (c) chemical reaction and variation of (d) Bejan number with the particle diameter, for an upward flow configuration at different freestream velocities and a freestream temperature of 300 K, under normal gravity.

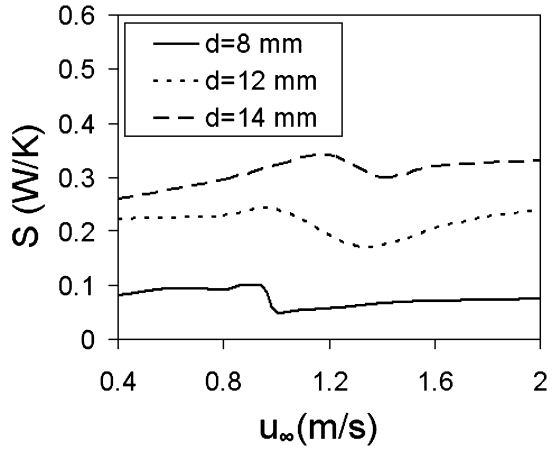

Fig. 14. Variation of the total entropy generation rate over the volume ($\mathrm{W\,K^{-1}}$) with freestream velocity, for an upward flow configuration with freestream temperature of 300 K, for different particle diameters under normal gravity.

ambient temperature (solid and dotted lines in Fig. 12(b)), and this trend is also reported in Ref. [27].

3.3. Effect of particle size

The particle diameter has been varied from 8 mm to 18 mm. An upward flow configuration under normal gravity with an ambient temperature of 300 K has been employed in the simulations. Freestream velocities have been varied from 0.2 $\mathrm{m\,s^{-1}}$ to 2 $\mathrm{m\,s^{-1}}$. Fig. 13 shows the variation of the entropy generation rate over the volume with the particle diameter, due to heat transfer (Fig. 13(a)), mass transfer (Fig. 13(b)) and chemical reaction (Fig. 13(c)), at various freestream velocities. Also, shown is the variation of Bejan number with the particle diameter (Fig. 13(d)). Overall, there is an increasing trend in the entropy generation rates with the particle diameter. This is consistent with the report in the literature [25]. For certain combinations of freestream velocity and particle diameter, the variation of the entropy generation rate with particle diameter becomes highly non-linear (for example, dashed line in Fig. 13(b)). The decreasing trend observed in the variation of Bejan number (Fig. 13(d)), shows that as the particle diameter increases, the contribution to the total entropy generation rate due to heat transfer decreases.

Fig. 14 shows the variation of the total entropy generation rate integrated over the volume, with the freestream velocity for different particle diameters. This consolidates the results presented in Fig. 13. The increasing trend in the entropy generation rate with particle diameter is clearly seen. Also, for larger particles, since flame transition takes place at a higher freestream velocity, decrease in the entropy generation rate is also observed at a higher freestream velocity.

In order to develop a correlation for entropy generation rate as a function of the freestream velocity, a non-dimensional total entropy generation number has been defined as follows:

Total entropy generation number

$$N_S = \frac{S}{\rho_\infty u_\infty d^2 C_{p\infty}}$$

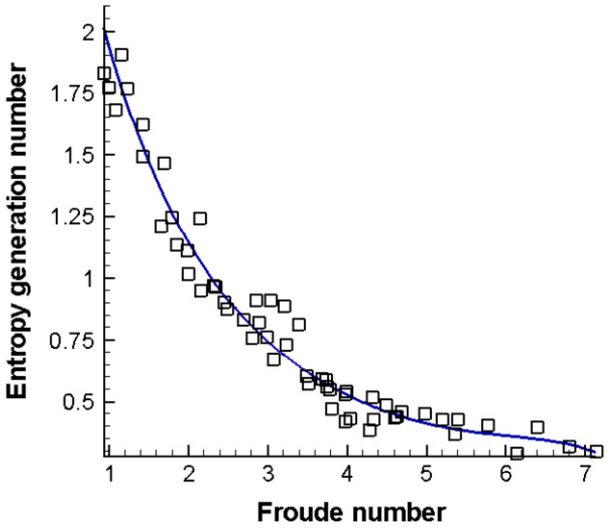

Fig. 15. Correlation for the total entropy generation number as a function of the Froude number, for upward flow configuration with freestream temperature of 300 K, under normal gravity.

For an upward flow configuration under normal gravity with an ambient temperature of 300 K, a fifth order polynomial fit has been plotted in Fig. 15 for the variation of the total entropy generation number (N_s) as a function of Froude number ($u_\infty/(gd)^{1/2}$) (solid line in Fig. 15). The choice of Froude number as the independent variable is due to the fact that flame transition occurs approximately at a unique Froude number ($Fr \sim 3.5$), irrespective of the particle diameters considered in this study. The symbols in the plot represent the scatter of the total entropy generation number with respect to the Froude number, when the particle diameter is varied from 8 mm to 18 mm and the freestream velocity from 0.2 $\mathrm{m\,s^{-1}}$ to 2 $\mathrm{m\,s^{-1}}$. The correlation could be employed to calculate the total entropy generation rate over the volume for methanol fuel particles burning in an upward flow configuration under normal gravity at an ambient temperature of 300 K.

4. Conclusions

Entropy generation during the quasi-steady combustion of spherical fuel particles has been presented in detail. The effects of freestream velocity, particle diameter, ambient temperature and gravity, on the entropy generation rate, have been discussed in detail. The major results are summarized below.

In the range of sub-critical freestream velocity, where an envelope flame is present, the entropy generation rate presents a minimum value. At the critical velocity, where flame transition occurs, entropy generation rate reaches a maximum value. Flame transition significantly affects the entropy generation rate and a sharp decrease is observed in entropy generation rate after the transition. In the super-critical range of freestream velocity, where a transition or a wake flame is present, there is an increasing trend for entropy generation rate. However, the maximum value of the entropy generation rate in the super-critical range is less than the minimum value noted in the sub-critical range.

Heat transfer and chemical reaction contribute almost equally to the total entropy generation rate followed by the contribution from mass transfer. The coupling between heat and mass transfer contributes very little. Contributions from fluid friction and body force are negligible.

When normal gravity is considered in an upward flow configuration, in which the buoyancy-induced flow adds to the forced convective flow, there is an increase in the entropy generation rate when compared to the zero gravity case. However, the effect of gravity poses a complex pattern in the entropy generation rate for a downward flow configuration in which buoyancy effects opposes the forced convection.

An increase in the ambient temperature, in general, results in a decrease of the total entropy generation rate, even though the entropy generation rate due to mass transfer increases with ambient temperature. However, at an intermediate ambient temperature, variation in the entropy generation rates become quite complex.

As the particle diameter is increased, entropy generation rate also increases. Decreasing trend is observed in the variation of Bejan number, which shows that as the particle diameter increases, the contribution to the total entropy generation rate due to heat transfer decreases. A correlation has been presented for the non-dimensional entropy generation number as a function of Froude number, for a particle burning in an upward flow configuration under normal gravity with an ambient temperature of 300 K.

Appendix A. Numerical formulation and solution procedure

The governing equations are non-dimensionalized using appropriate length, velocity and time scales. The free stream velocity (u_∞) is chosen as reference velocity. The particle diameter d is used as reference length scale and the ratio of particle diameter to free stream velocity is used as the time scale. All the other variables have been made dimensionless by combining these three reference quantities with the appropriate free stream parameters. The dimensionless variables are listed below.

Coordinates:

$$x = \frac{x^*}{d}, \qquad r = \frac{r^*}{d}, \qquad t = \frac{t^* u_\infty}{d}$$

Flow variables:

$$u = \frac{u^*}{u_\infty}, \qquad v = \frac{v^*}{u_\infty}, \qquad \rho = \frac{\rho^*}{\rho_\infty}, \qquad p = \frac{p^*}{\rho_\infty u_\infty^2}$$

$$T = \frac{T^* - T_\infty}{T_\infty}, \qquad h = \frac{h^*}{C_{P_{\text{ref}}} T_\infty}$$

Transport variables and physical properties:

$$\mu = \frac{\mu^*}{\mu_{\text{ref}}} \frac{\mu_{\text{ref}}}{\rho_\infty u_\infty d} = \frac{\mu^*}{\mu_{\text{ref}}} \frac{1}{Re_\infty}, \qquad C_P = \frac{C_P^*}{C_{P_{\text{ref}}}}$$

$$D_{\text{im}} = \frac{D_{\text{im}}^*}{D_{\text{ref}}} \frac{D_{\text{ref}} \nu_{\text{ref}}}{\nu_{\text{ref}} u_\infty d} = \frac{D_{\text{im}}^*}{D_{\text{ref}}} \frac{1}{Re_\infty Sc_\infty}$$

$$k = \frac{k^*}{k_{\text{ref}}} \frac{k_{\text{ref}}}{\rho_\infty u_\infty C_{P_{\text{ref}}} d} = \frac{k^*}{k_{\text{ref}}} \frac{1}{Re_\infty Pr_\infty}$$

Rate of reaction:

$$\dot{\omega}_i = \frac{\dot{\omega}_i^* d}{\rho_\infty u_\infty}$$

Variables with the superscript * in the above equations denote dimensional quantities.

A.1. Governing equations

The dimensionless governing equations for mass, momentum, species and energy conservation in the gas phase are given below in flux form for each control volume cell, in cylindrical polar coordinates.

(1) x-momentum equation

$$\frac{\mathrm{d}}{\mathrm{d}t}(\rho u) V_{\text{cell}} + \oint \rho u (u n_x + v n_r) 2\pi r \,\mathrm{d}l = \oint (\sigma_{xx} n_x + \tau_{rx} n_r) 2\pi r \,\mathrm{d}l + \frac{1}{Fr^2}\left(1 - \frac{\rho}{\rho_\infty}\right) V_{\text{cell}} \tag{A.1}$$

where, V_{cell} is the volume of the cell and Fr is the Froude number.

(2) r-momentum equation

$$\frac{\mathrm{d}}{\mathrm{d}t}(\rho v) V_{\text{cell}} + \oint \rho v (u n_x + v n_r) 2\pi r \,\mathrm{d}l = \oint (\tau_{rx} n_x + \sigma_{rr} n_r) 2\pi r \,\mathrm{d}l - \frac{\sigma_{\theta\theta}}{r} V_{\text{cell}} \tag{A.2}$$

The stress terms in the above equations can be written as:

$$\sigma_{xx} = -p + 2\frac{\mu}{\mu_{\text{ref}}} \frac{1}{Re_\infty} \frac{\partial u}{\partial x}$$

$$\sigma_{rr} = -p + 2\frac{\mu}{\mu_{\text{ref}}} \frac{1}{Re_\infty} \frac{\partial v}{\partial r}$$

$$\sigma_{\theta\theta} = -p + 2\frac{\mu}{\mu_{\text{ref}}} \frac{1}{Re_\infty} \frac{v}{r}$$

$$\tau_{rx} = \tau_{xr} = \frac{\mu}{\mu_{\text{ref}}} \frac{1}{Re_\infty} \left(\frac{\partial u}{\partial r} + \frac{\partial v}{\partial x}\right)$$

(3) Species conservation equation

Here a global single step reaction with 5 species (Fuel, oxygen, CO_2, H_2O, N_2) has been considered. For a particular species "i", the species conservation equation is of the form,

$$\frac{\mathrm{d}}{\mathrm{d}t}(\rho Y_i) V_{\text{cell}} + \oint \rho Y_i (u n_x + v n_r) 2\pi r \,\mathrm{d}l = \oint \rho \frac{D_{\text{im}}}{D_{\text{ref}}} \frac{1}{Re_\infty Sc_\infty} \left(\frac{\partial Y_i}{\partial x} n_x + \frac{\partial Y_i}{\partial r} n_r\right) 2\pi r \,\mathrm{d}l + \dot{\omega}_i V_{\text{cell}} \tag{A.3}$$

with $\overset{*}{\omega}_i$ denoting the mass rate of production of species i per unit volume.

(4) Energy conversation equation

The energy conservation equation in flux form is given by,

$$\frac{\mathrm{d}}{\mathrm{d}t}(\rho C_P T)V_{\mathrm{cell}} + \oint \rho C_P T(un_x + vn_r)2\pi r\,\mathrm{d}l = \frac{1}{Re_\infty Pr_\infty}\left(\oint \frac{k}{k_{\mathrm{ref}}}\left(\frac{\partial T}{\partial r}n_r + \frac{\partial T}{\partial x}n_x\right)2\pi r\,\mathrm{d}l\right) - \sum_{i=1}^{n}\dot{\omega}_i h_{fi} V_{\mathrm{cell}} + \left(\sum_{i=1}^{n}\oint \rho \frac{D_{\mathrm{im}}}{D_{\mathrm{ref}}}\frac{1}{Re_\infty Sc_\infty} \times C_{Pi}T\left(\frac{\partial Y_i}{\partial r}n_r + \frac{\partial Y_i}{\partial x}n_x\right)2\pi r\,\mathrm{d}l\right) \quad (A.4)$$

In the above equation h_{fi} is the enthalpy of formation for ith species.

A.2. Solution procedure

The governing equations have been discretized using the finite volume method. A non-orthogonal grid with semi-collocated, four noded quadrilateral cells has been employed for the numerical calculations [15,34]. Within each non-orthogonal cell, the variables are interpolated with general bilinear interpolation functions, used commonly in finite element method [12]. A brief description of the solution procedure is given here. Details of the evaluation of fluxes and derivatives and discretization of the integral form of governing equations are available elsewhere [15,34].

The velocity components are obtained by integrating the momentum equations, using an explicit time marching scheme with an assumed pressure field $\tilde{p}$. These velocities will usually not satisfy the continuity equation. Hence, the mass residue for each continuity cell is evaluated and the associated pressure corrections are obtained by solving the pressure Poisson equation of the form:

$$\nabla^2 p' = \frac{\rho}{\Delta t}\left(\frac{\partial u}{\partial x} + \frac{1}{r}\frac{\partial}{\partial r}(rv)\right)$$

where, the right-hand side term represents the continuity equation residue. After integrating the pressure correction equation over the continuity cells, the resulting pressure gradient terms across the cell boundaries are evaluated using the general interpolation schemes, to yield a set of simultaneous algebraic equations in terms of p'. The cell pressures are then updated as $p^{n+1} = \tilde{p} + p'$ and the velocities are also updated by solving the momentum equations again with the updated pressure field.

Mass fraction equations and the energy equation are solved using the explicit time marching scheme with a smaller time step value for a certain number of inner iterations. The thermophysical properties are updated using empirical relations [15, 34]. The chemical kinetic equation is solved to obtain the reaction rate at the updated temperature. This transient marching procedure is carried out until either the steady state or a time independent oscillatory solution is obtained. For the finite rate chemistry model, initially, a certain number of iterations are carried out (for flow solution alone) without solving the energy and reaction rate equations. After obtaining the cold flow solution, a suitable high temperature region is then patched near the particle, so that ignition can occur followed by combustion. Then, by time marching, the complete set of equations is solved.

The solution methodology outlined above has been implemented using a FORTRAN code and computations have been carried out on Intel Pentium III processor based Personal computers, SGI workstations and HP cluster machines. A grid sensitivity study with 16 000, 22 000 and 32 000 cells has shown that a grid with 22 000 cells gives a good balance between computational economy and solution accuracy for a wide range of parameters considered in the present study. For most of the cases, the time step size is 1.0e–05 seconds and it takes about 30 000 time steps to have either a converged solution or obtain enough cycles in the unsteady solution. Each computation required about 10 hours of wall clock time on the Pentium based PCs.

References

[1] H.S. Caram, N.R. Amundson, Diffusion and reaction in a stagnant boundary layer about a carbon particle, Industrial Engineering Chemistry Fundamentals 16 (2) (1977) 171–181.

[2] E. Mon, N.R. Amundson, Diffusion and reaction in a stagnant boundary layer about a carbon particle. 2. An extension, Industrial Engineering Chemistry Fundamentals 17 (4) (1978) 313–321.

[3] M.K. King, Ignition and combustion of boron particles and clouds, Journal of Spacecraft 19 (4) (1982) 294–306.

[4] H. Isoda, S. Kumagai, Combustion of fuel droplets in a falling chamber, in: Sixth Symposium (International) on Combustion, The Combustion Institute, 1955, pp. 726–731.

[5] A. Chervinsky, Transient burning of spherical symmetric fuel droplets, Israel Journal of Technology 7 (1969) 35–42.

[6] S. Kumagai, T. Sakai, S. Okajima, Combustion of free fuel droplets in a freely falling chamber, in: Thirteenth Symposium (International) on Combustion, The Combustion Institute, 1971, pp. 779–785.

[7] H. Sami, M. Ogasawara, Study on the burning of a fuel drop in heated and pressurized air stream, JSME Bulletin 13 (1970) 395–426.

[8] S.R. Gollahalli, T.A. Brzustowski, Experimental studies on the flame structure in the wake of a burning droplet, in: Fourteenth Symposium (International) on Combustion, The Combustion Institute, 1973, pp. 1333–1344.

[9] H.A. Dwyer, B.R. Sanders, A detailed study of burning fuel droplets, in: Twenty-First Symposium (International) on Combustion, The Combustion Institute, 1986, pp. 633–639.

[10] S.Y. Cho, R.A. Yetter, F.L. Dryer, A computer model for one-dimensional mass and energy transport in and around chemically reacting particles, including complex gas-phase chemistry, multi-component molecular diffusion, surface evaporation and heterogeneous reaction, Journal of Computational Physics 102 (1992) 160–168.

[11] P. Balakrishnan, T. Sundararajan, R. Natarajan, Interference effects during burning of tandem porous spheres in mixed convective environment, AIAA Journal 38 (2000) 1889–1898.

[12] P. Balakrishnan, T. Sundararajan, R. Natarajan, Combustion of a fuel droplet in a mixed convective environment, Combustion Science and Technology 163 (2001) 77–106.

[13] D.N. Pope, G. Gogos, A new multi-component diffusion formulation for the finite volume method: application to convective droplet combustion, Numerical Heat Transfer Part B 48 (3) (2005) 213–234.

[14] D.N. Pope, G. Gogos, Numerical simulation of fuel droplet extinction due to forced convection, Combustion and Flame 142 (2005) 89–106.

[15] V. Raghavan, V. Babu, T. Sundararajan, R. Natarajan, Flame shapes and burning rates of spherical fuel particles in a mixed convective environment, International Journal of Heat and Mass Transfer 48 (2005) 5354–5370.

[16] J.O. Hirschfelder, C.F. Curtiss, R.B. Bird, Molecular Theory of Gases and Liquids, Wiley, New York, 1954.

[17] A. Bejan, Advanced Engineering Thermodynamics, Wiley, New York, 1988.
[18] A. Bejan, Second law analysis in heat transfer, Energy 5 (1980) 721–732.
[19] A. Bejan, Entropy Generation through Heat and Fluid Flow, Wiley, New York, 1982.
[20] A. Bejan, The thermodynamic design of heat and mass transfer processes and devices, International Journal of Heat and Fluid Flow 8 (1987) 258–276.
[21] J.Y. San, W.M. Worek, Z. Lavan, Entropy generation in convective heat transfer and isothermal convective mass transfer, Transaction of the ASME, Journal of Heat Transfer 109 (1987) 647–652.
[22] V.S. Arpaci, A. Selamet, Entropy production in flames, Combustion and Flame 73 (1988) 251–259.
[23] S.K. Dash, S.K. Som, Transport processes and associated irreversibilities in droplet combustion in a convective medium, International Journal of Energy Research 15 (7) (1991) 603–619.
[24] I.K. Puri, Second law analysis of convective droplet burning, International Journal of Heat and Mass Transfer 35 (10) (1992) 2571–2578.
[25] S. Hiwase, A. Datta, S.K. Som, Entropy balance and exergy analysis in the process of droplet combustion, Journd of Physics D. Applied Physics 31 (1998) 1601–1610.
[26] A. Datta, S.K. Som, Thermodynamic irreversibilities and second law analysis in a spray combustion process, Combustion Science and Technology 142 (1999) 29–54.
[27] A. Datta, Entropy generation in a confined laminar flame, Combustion Science and Technology 159 (2000) 39–56.
[28] K. Nishida, T. Takagi, S. Kinoshita, Analysis of entropy generation and exergy loss during combustion, in: Twenty-ninth Symposium (International) on Combustion, The Combustion Institute, 2002, pp. 869–874.
[29] H. Yapici, G. Basturk, N. Kayatas, B. Albayrak, Numerical study of effect of oxygen mass fraction on local entropy generation in a methane–air burner, Sādhanā 29 (6) (2004) 641–667.
[30] A. Datta, Effects of gravity on structure and entropy generation of confined laminar diffusion flames, International Journal of Thermal Sciences 44 (2005) 429–440.
[31] V. Raghavan, G. Gogos, V. Babu, T. Sundararajan, Effect of gravity on methanol diffusion flames burning within a forced convective environment, International Communications in Heat and Mass Transfer 33 (2006) 686–697.
[32] R.C. Reid, J.M. Prausnitz, B.E. Poling, The Properties of Gases and Liquids, McGraw-Hill book Company, New York, 1986.
[33] R.S. Turns, An Introduction to Combustion: Concepts and Applications, McGraw-Hill Book Company, New York, 2001.
[34] V. Raghavan, Modeling of unsteady effects during spray droplet burning, PhD thesis, Indian Institute of Technology Madras, Chennai, India, 2004.